BILINGUAL PUBLISHING CO.
Pioneer of Global Academics Since 1984

Journal of Metallic Material Research
https://ojs.bilpublishing.com/index.php/jmmr

ARTICLE

Hot Cracking Susceptibility of 800H and 825 Nickel-Base Superalloys during Welding via Spot Varestraint Test

Chih-Chun Hsieh[1,*] Ching-Yi Pao[2] Weite Wu[2]

1. Department of Aircraft Engineering, Air Force Institute of Technology, No.1, Julun Rd., Gangshan Dist., Kaohsiung City 820, Taiwan
2. Department of Materials Science and Engineering, National Chung Hsing University, 145 Xingda Rd. Taichung 402, Taiwan

ARTICLE INFO

Article history
Received: 24 February 2019
Accepted: 15 March 2019
Published Online: 19 April 2019

Keywords:
Gas tungsten arc welding
Hot cracking sensitivity
Nickel-base superalloys
Heat-affected zone

ABSTRACT

Hot cracking susceptibility of fillers 52 and 82 in 800H and 825 nickel-base superalloys was discussed using the Spot Varestraint test. The fillers of 52 and 82 were added into nickel-base superalloys via a gas tungsten arc welding (GTAW).Experimental results showed that the hot cracking sensitivity of the nickel-base superalloys with filler at high temperature was lower than that without filler. The hot cracking sensitivity had a slight effect when the filler 82 was added. The total length of crack was increased, the liquid-solid (L-S) two-phase range is higher so that the hot cracking susceptibility will be raised. The morphologies of cracks included the intergranular crack in the molten pool, molten pool of solidification cracking, heat-affected zone of intergranular cracks, and transgranular crack in the heat-affected zone.

1. Introduction

The cracks of the components often been occurred in the aerospace industry under high temperature corrosion and strain environments so that the industrial loss and casualty [1-3]. In the early 1960s, Kammer et al. [4] separated weld cracks into two categories: hot cracking and cold cracking. When cracks occurred near the solidification temperature, they were called hot cracks. Also, Hemsworth et al. [5] classified high-temperature weld cracks for both single-and multipass welds. The two main categories were segregation cracking (including solidification and liquation cracking) and ductility-dip cracking. Other studies have suggested cracks have resulted from high temperatures during reheating in multipass welding, repair welding, or postweld annealing; all of these are known as reheat cracking. Hot cracking in welding applications or experiments appears in stainless steels, Al alloys, superalloys, carbon steels, alloy steels, Ti alloys, and Cu alloys. Hot cracking occurs in the base material's heat-affected zone (HAZ) or in the weld itself. The failure mode is intergranular.

Some harmful secondary phase (Such as: σ phase, μ phase, and Laves phase) can be precipitated in nickel alloys if the chemical composition cannot be controlled during the heat treatment. These precipitate phases can decrease the fracture strength and ductility and then cause the cracks [6-8].

**Corresponding Author:*
Chih-Chun Hsieh,
Department of Aircraft Engineering, Air Force Institute of Technology, No.1, Julun Rd., Gangshan Dist., Kaohsiung City 820, Taiwan;
Email: 1106010@gwolian.com

 DOI: https://doi.org/10.30564/jmmr.v2i1.958

In this study, the hot cracking susceptibilityin different nickel alloys of 800H, 825, 800H-52, 800H-82, 825-52, and 825-82 was investigated using the GTAW welding. A series of equipment was used to discuss the crack mechanism, such as the Varestraint test, optical microscope (OM), scanning electron microscope (SEM), X-ray diffractometer (XRD), and differential scanning calorimetry (DSC). The solidus temperature (T_S) and liquidus temperature (T_L) can be measured via the Differential Thermal Analysis and calculate the solidus-liquidus difference value (ΔT). The ΔT index was used to evaluate the hot cracking susceptibility in this study.

2. Experimental Procedures

The 800H and 825 nickel-base superalloys were welded using the gas tungsten arc welding (GTAW). The welding was performed with Nickel filler metals of 82 and 52 and welded on 800H and 825 Nickel alloys. The spot welding was carried out and hot cracking was estimated using the Spot Varestraint machine (see Figure 1). The welded samples were used to observe the microstructures, composition, macrostructures, average amount, average length, and maximum length.

The Incoloy 800H and Incoloy 825 were used for the experimental substrates and specimen size was 200 mm × 50 mm × 5 mm. The Incoloy 82 (#82) and Incoloy 52 (#52) were selected for the filler metals and their diameters were 1.2 mm. The detailed composition was listed in Table 1. The groove types can be divided into the grooved and not grooved specimen. The grooved sample was a single V-Groove with 90^o and a distance between an oblique angle and bottom was 1 mm. The same positions were taken for the welded sample with filler and without filler. The top and bottom parts were ground to 1 mm and final sample thickness was 3 mm. The best welding parameters of the filler welding and Spot Varestraint test were determined as shown in Tables 2 and 3.

The relationship between applied strain and crack length were discussed by Varestraint test and evaluate the hot cracking susceptibility [9-11]. The crack in the HAZ and fusion zone (FZ) was estimated using the SOB (Spot on Bead) test [12-16]. The Argon welding gun moved from left to center during test and the mold block of specific curvatureradius is under the sample.

Both ends of the specimen were extruded via an oil pressure arm and then the center points of specimen were bent. Hence, the surface of specimen formed a strain (ε), as indicated as Equation 1:

$$\varepsilon(\%)=t/2/R \quad (1)$$

where ε: The strain in the surface

t: The thickness of specimen

R: The curvature radius of the mold block

The relationship between the amount of crack and the crack length were observed using the Stereo binocular microscope after Spot Varestraint test.

The composition in the matrix and welds was analyzed using the Spark discharge spectrometer. Five measured points were taken in smooth sample surface. Finally, an average value was calculated.

For the Spot Varestraint specimen, the observation regions had three parts of center, solidified zone, HAZ in order to analysis the hot cracking susceptibility. The specimen were divided into 20 portions were observed using the Stereo binocular microscope.

Three observed directions of can be divided into the normal direction (ND), tangential direction (TD), and welding direction (WD) in the welds (see Figure 2), and cut the rolled samples into a suitable size using a precision cutting machine. And then mounted by molding epoxy, then ground using #100~#200 SiC papers and polished with 0.05 μm Al_2O_3 powder paste. The Aqua regia plus Glycerin was used as an etchant for 60 seconds. Finally, the samples of the substrate and welds were observed using the optical microscope (ZEISS Axioskop 2 MAT, OM).

An X-ray diffractometer (Siemens D5000, XRD) with Cu Kα radiation was utilized to analyze the effect of precipitates on hot crack in the substrate and welds at a scanning rate of 2^o/min and a 2θ value from 20^o to 100^o.

The relationship between precipitates of hot crack and filler were discussed using a Field Emission Scanning Electron Microscope (JSM-6700F JEOL, FESEM). The elemental analysis of the TiN or other precipitates were performed by using an Energy Dispersive Spectrometer (EDS).

Hardness of the substrate, HAZ, and welds were measured by a Vickers hardness tester with a 300 g load for 10 seconds at a quarter plane from the specimen surface.

The 800H, 825, 800H-52 (with #52 filler), 800H-82 (with #82 filler), 825-52 (with #52 filler), and 825-82 (with 82 filler)were sampled within 100 mg and analyzed thethermal reactions using the Differential Thermal Analysis (STA PT 1600 Linseis, DTA). The experimental temperature range is between 1273K(1000^{o}C) and 1773K(1500^{o}C) with a heating rate of 275K(2°C)/min. The solidus temperature (T_S), liquidus temperature (T_L), solidus-liquidus coexistent zone(ΔT) can be measured via the DTA. Above indexes can be used to evaluate the hot cracking susceptibility.

DOI: https://doi.org/10.30564/jmmr.v2i1.958

3. Results and Discussion

3.1 Microstructural Observation

Figure 3 showed the metallographic microstructures in the matrixes of the 800H and 825 alloys. Two alloys indicated different equiaxed grains and theirs growth direction had no fixed direction. From the EDS analysis, the inner grains and polygonal particles were identified as the TiN precipitates. The 800H and 825 are the Fe and Ni solution strengthening nickel alloys and had many annealing twins. The microstructures exhibited bigger grains in 800H alloys than that in 825 alloys. Therefore, it showed bigger TiN precipitates in 800H alloys. The cooling time can affect the grain size at the final step of the solution treatment. The grains had enough time to nucleate and grow under a sufficient cooling time. The big size TiN grains will be formed.

Figures 4-6 showed the metallographic microstructures of the ND, TD, and WD of the welds in 800H-52 filler, 800H-82 filler, 825-52 filler, and 825-82 filler, respectively. The results indicated that no TiN precipitate existed in the welds of four nickel alloys. This is because that the high cooling rate leads to high temperature gradient so that the columnar and dendritic structures are formed.

Microstructure development of four alloys fillers (800H-52, 800H-82, 825-52, and 825-82) from a fusion boundary to a center was planar →columnar dendrite → equiaxed dendrite. The difference of these microstructures is from the temperature gradient. The temperature loss in fusion boundary is lower than that in the center so that the microstructure in fusion boundary indicated the planer structure. Furthermore, the cooling rate is higher in the center than that in other regions so that the microstructure showed the equiaxed grains.

3.2 X-ray Diffraction Analysis

Figure 7 showed the XRD results of the welds in 800H, 825, 800H-82, and 825-82 alloys. Results indicated that the Ni-Cr-Fe phase was found in these alloys. This phase was identified as a FCC γ-phase. However, no second phase was examined from diffraction patterns, e.g. $M_{23}C_6$, σ phase, or other low melting point phase. This is because that the grain size of the carbides or other precipitates was small so that XRD cannot detect them.

3.3 Micro hardness Analysis

Figure 8 showed the Vickers hardness on the surface of the 800H, 825, 800H-52, 800H-82, 825-52, and 825-82. The hardness in 800H alloy was lower than that in 825 alloy. The 800H and 825 alloys are the Fe and Ni solution strengthening alloys. In general, two alloys should indicate a similar hardness value. However, the grain size in 825 alloys was smaller than that in 800H alloys from the microstructural observation attributed to an effect of grain refinement strengthening. According to the EDS results, lots of the TiN precipitates were found in the surface of alloys.

3.4 Thermal Analysis

Figure 9 showed the exothermic curves of the 800H, 825, 52 alloy filler, 82 alloy filler, 800H-52, 800H-82, 825-52, and 825-82. The liquidus temperatures (T_L) in 800H, 800H-52, 800H-82, 825, 825-52, 825-82, 52 filler, and 82 filler were 1709K(1436°C), 1676K(1403°C), 1651K(1378°C), 1654K(1381°C), 1671K(1398°C), 1637K(1364°C), 1669K(1396°C), and 1561K(1288°C), respectively. The temperature difference of residual liquid during the solidification can be represented as an index of the ΔT ($T_L - T_S$). The T_L and T_S are the liquidus temperature and solidus temperature. When the value of the ΔT is higher, residual liquid will be kept a long time at high temperature and then lose the strength of grain boundaries during coolingshrinkage. Consequently, the hot cracking will happen. No phase transformation was detected from the thermal analysis and then thesingle stabilizeγ-phase was found in the nickel alloys from the XRD analysis. Table 4 showed the thermal analysis results of the nickel alloys. These ΔT values can be used to predict the hot cracking susceptibility in the nickel alloys. The order of hot cracking susceptibility of the nickel alloys was (a): 800H>800H-52>800H-82; (b): 825-52>825-82>825.

3.5 The Crack Analysis

Fig 10 showed the macrostructure observation of the cracks in 800H, 825, 800H-52, 800H-82, 825-52, and 825-82 alloys. The crack observation was performed using the spot welding via a Spot Varestraint test. The critical strain of experimental samples can be increased rapidly after the spot welding and it can equalize the critical strain and crack strain. Then, the crack will be expanded along the fusion boundary. The distribution of the cracks can be divided into four regions of the center zone (CZ), FZ, partial melted zone (PMZ), and HAZ, as shown in Figure 11. The arc shear stress occurs during the welding and the surface tension exists in the center of the FZ because the center zone is close to the welding gun. The concaveshrinkage can be observed in the center zone and longer and deeper cracks can be formed in this region. However, the dendritic microstructures were found in the FZ. The residual liquids can backfill the cracks during the solidification

 DOI: https://doi.org/10.30564/jmmr.v2i1.958

so that this region has no obvious macro-crack. The PMZ is the closest region of the fusion boundary. This region indicated the semi-fused liquid and the poor liquidity and a little residual liquid under high temperature. Consequently, it cannot backfill the cracks in the PMZ.

The cracks can be divided into two parts of (a) dendritic solidification crack in center zone and (b) low ductility crack in HAZ, as shown in Figure 12. The temperature difference of solid and liquid was small during solidification in welding pool and in center zone so that backfill of the residual liquid was not enough. Therefore, the solidification crack can occur during cooling because of shrinkage. The liquation film will be formed in the grain boundary if the low melting point phase precipitates in the dendrite and the HAZ. Hence, the liquation film crack will be occurred. In this study, no low melting point phases at high temperature were detected from the DTA analytical results. The formation mechanism of the cracks should be a low ductility crack. When a liquid is solidified into a solid during the solidification, the low ductility in the HAZ and high strain during thermal expansion and contraction will lead to the intergranular crack.

3.6 The Amounts of Cracks

The average amounts of cracks were shown in Figure 13. The amount measurement of crack can divide into three regions of the center zone, FZ, HAZ plus PMZ (HAZ+PMZ). The crack length of the center zone in 800H alloy was the longest and obvious. However, the crack length of the crack of the center zone in 825-82 alloy was the shortest and unobvious. The order of crack amount in the center zone was 800H>800H-52>800H-82 and 825>825-82>825-52. However, that in the FZ was 800H>800H-52>800H-82 and 825>825-82>825-52. Furthermore, that in the HAZ+PMZ was 800H>800H-52>800H-82 and 825>825-52>825-82. From the amount of cracks and thermal analyses, the results of the crack amount and the ΔT value in the HAZ+PMZ indicated the same tendency. When the ΔT value increases, the amount of cracks will be increased.

3.7 Total Length of the Cracks

Figure 14 showed the total length of the cracks in the nickel alloys of the center zone, PMZ+HAZ, and FZ. The total crack length (TCL) can be used to examine the hot cracking susceptibility. Generally, the amounts of the cracks were higher; the total length of the cracks was longer. The order of total length of the cracks in the center zone was 800H>800H-82>800H-52 and 825-82>825>825-52. On the other hand, that in the FZ was 800H>800H-82>800H-52 and 825-82>825-52>825. Besides, that in the HAZ+PMZ was 800H>800H-52>800H-82 and 825>825-52>825-82. The total length of the crack in 800H alloy was the longest of the all nickel alloys so that the ΔT value was highest in 800H alloy. Consequently, the hot cracking susceptibilityin 800H was more evident.

The crack analyses indicated the same tendency of the hot cracking susceptibility (800H>800H-52>800H-82; 825>825-52>825-82) in the HAZ+PMZ of the all nickel alloys. The hot cracking susceptibility was the highest in the 800H and 825 alloys without filler addition. However, the hot cracking susceptibility can be decreased with filler addition. Because the ΔT value in the 800H alloy was high so that the hot cracking susceptibility was more obvious. Although the ΔT value in the 825 alloys was smaller than that in the 800H alloys, the hot cracking susceptibility in the 825 alloys was higher than that in the containing filler nickel alloys. Above results were because of following two reasons: (a) The grain size in matrix; (2) The dendrite in the surroundings of the welds during welding. For a bigger grain, the intergrain is easy to slip under high temperature strain and then the cracks grow easily, as shown in Figure 15(a). For a smaller grain, the intergrain is difficult to slip under high temperature strain and the growth of the cracks was retarded, as shown in Figure 15(b). However, many dendritic structures in the welds with filler suppressed the mobility of the dendrite arms and then the propagation of the cracks became difficult, as indicated in Figure 15(c). Therefore, the hot cracking susceptibility in the 825 alloys with 52 and 82 fillers can be decreased because of the interaction between dendrite arms.

3.8 Microstructures in the Surface of the Cracks

Figures 16-17 showed the microstructural distribution of the Varestraint test. Figures 16(a) and 17(a) were microstructures of the HAZ and had some annealing twins and smaller black points of the TiN precipitates in the grained structures. However, the microstructures indicated a planar growth if the filler was added into the matrix. Figures 16(b) and 17(b) were microstructures of the partial melted zone (PMZ) and the microstructures were similar to the FZ. This region was a like-planar growth and every planewas different direction growths. Figures 16(c) and 17(c) showed the microstructures of the FZ and this region exhibited a dendritic growth. It closed to the center area and had an obvious temperature gradient so that the dendritic growth was observed. Figures 16(d) and 17(d) were microstructures of the center zone and the microstructures were the equiaxed structures under high temperature difference.

DOI: https://doi.org/10.30564/jmmr.v2i1.958

Figure 18 showed the metallographic observation of the crack in the nickel alloys and Figure 19 indicated the schematic diagram of different crack modes. Figure 19(a) was a crack in the FZ and high temperature difference led to the dendritic growth. The residual liquid does not backfill the crack completely so that the crack expanded along the two sides of dendrites. The residual liquid will be concentrate on the dendrites. Hence, the cracks were formed in above region under a critical deformation of the Varestraint test. Figure 19(b) showed the transgranular crack in the HAZ. The matrix without filler addition was located in this region. It does not form a weak region for residual liquid in the dendrites and grains so that the transgranular crack can be occurred directly. Figure 19(c) was a crack with filler addition and the cracks were expanded in this area along the dendritic boundaries. The boundaries of different directions were weak so that the dendritic boundaries were beneficial region to form the cracks. Figure 19(d) exhibited the cracks for a planar growth in the partial FZ. The orientation in the partial zones was very random and the strength in the grains was low so that the cracks were formed easily along the grain boundaries.

Figure 20 showed the SEI and BEI micrographsin the starting and terminal points of the cracks of 800H-52 alloys. The observed result is the same as Figure 19(d) and the starting point of the crack was formed along the grain boundaries of different directions. The terminal point of the crack was similar to the Figure 19(b). No residual liquid can expand the cracks so the growth mode of crack was a transgranular crack. The compositional results were indicated in Table 5. Figure 20(a) indicated that the composition in the starting point issimilar to that in the grains. Furthermore, lots of the TiN precipitates in the cracks of the terminal point HAZ. Figure 20(b) showed that the BEI micrograph for a starting point and a terminal point of the cracks. There were no harmful precipitates for cracks in the starting point and terminal point. Hence, the formation of the cracks had no relationship with the Al phase, Ti phase, B phase, P phase, S phase, γ' phase, Laves phase, and carbide whether fillers addition or not 800H and 825.

4. Conclusions

(1) The order of hot cracking susceptibility in nickel-basesuperalloys of 800H and 825during welding was 800H>800H-52>800H-82 and 825>825-52>825-82, respectively. The hot cracking susceptibility in the 825-82 alloy was the poorest of the all nickel alloys.

(2) When the 52 and the 82 fillers were added into the 800H and 825 alloys, the ΔT value will be decreased. The order of theΔT value in nickel alloys was 800H>800H-52>800H-82 and825-52>825-82>825, respectively.

(3) The solidification crack expanded along the grain boundaries or orientation grains and the growth mode of crack is the transgranular crack in the HAZ.

Acknowledgements

The authors are obligated to thank the Ministry and Science and Technology (MOST) of the Taiwan, R.O.C. for the financial support under the projects numbered MOST 103-2218-E-005-002.

Supplements

Table 2. Welding parameters of filler welding

Torch speed	120mm/min
Voltage	14V
Current	180A
Wire speed	193cm/min

Table 3. Welding parameters of Spot Varestraint test

Voltage	17.6V
Current	122A
Augmented Straint Range	5%
Under the push interval	0.1s
Welding time	3s

Table 4. Thermal analysis results of nickel alloys

	T_L(degree)	T_S(degree)	ΔT(degree)
800H	1436.4	1414.9	21.5
825	1381.0	1377.7	3.3
Filler 82	1288.1	1284.6	3.5
Filler 52	1396.4	1392.3	4.1

Table 1. Chemical composition of experimental materials

	Ni	C	Fe	Cr	Cu	Mo	Co	W	Mn	Al	Nb	Ti	Si
800H	31.24	0.102	45.94	19.89	0.020	0.304	0.023	0.642	1.07	0.447	0.093	0.385	0.177
825	40.19	0.025	31.51	20.80	2.775	3.442	0.000	0.102	0.583	0.090	0.118	0.526	0.204
#82	73.40	0.05	0.61	19.95	-	-	-	-	2.88	-	-	0.40	0.09
#52	58.50	0.03	9.60	28.90	-	-	-	-	0.26	0.57	-	0.55	0.24

 DOI: https://doi.org/10.30564/jmmr.v2i1.958

800H-52	1402.8	1399.6	3.2
800H-82	1377.9	1375.1	2.8
825-52	1397.7	1390.9	6.8
825-82	1363.9	1359.5	4.4

Table 5. EDS analysis of surrounding the cracks

Point	Element (wt%)				
	Cr	Fe	Ni	Ti	N
a	24.42	28.33	47.25	-	-
b	24.34	26.91	48.76	-	-
c	12.36	44.11	44.09	-	-
d	-	-	-	36.53	63.47

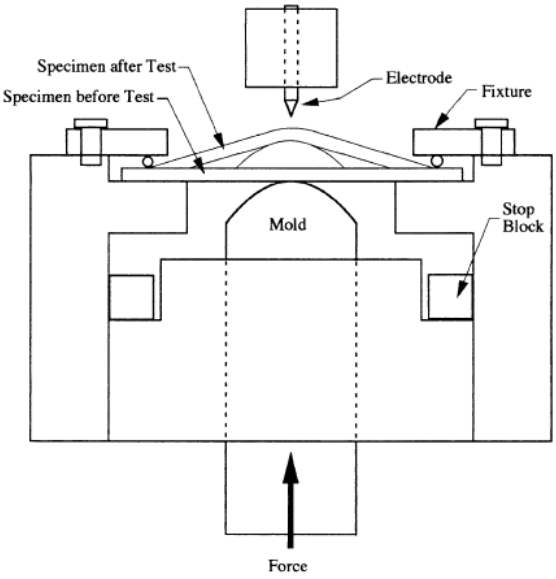

Figure 1. Spot Varestraint test apparatus

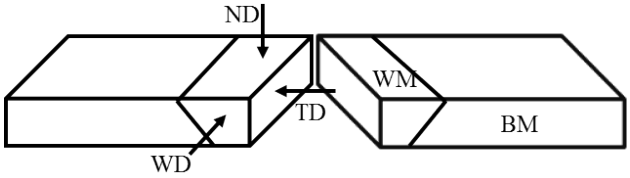

Figure 2. Definition of regions for microstructural observation

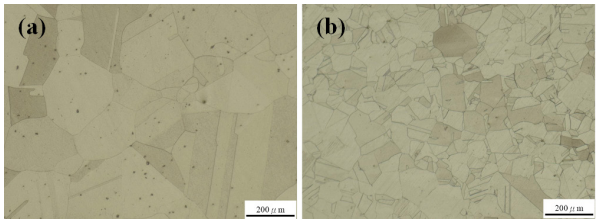

Figure 3. Metallographic microstructures of nickel-base-superalloys

Note: (a) 800H (b) 825 with an etchant of the Aqua regia plus Glycerin

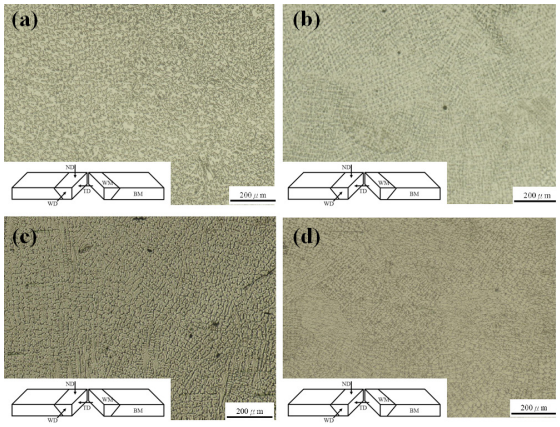

Figure 4. Microstructures of nickel-basesuperalloys in normal direction (ND)

Note: (a) 800H-52 (b) 800H-82 (c) 825-52 (d) 825-82 with an etchant of the Aqua regia plus Glyce

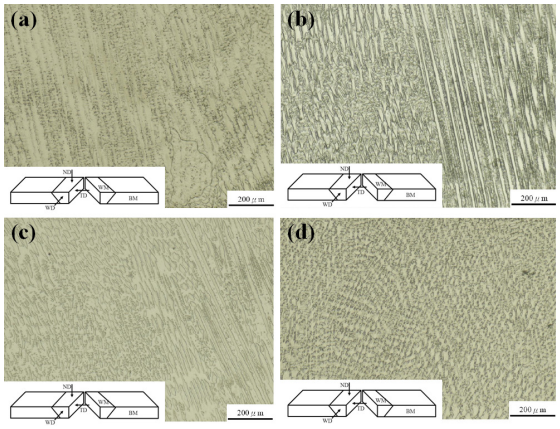

Figure 5. Microstructures of nickel-basesuperalloys in tangent direction (TD)

Note: (a) 800H-52 (b) 800H-82 (c) 825-52 (d) 825-82 with an etchant of the Aqua regia plus Glycerin

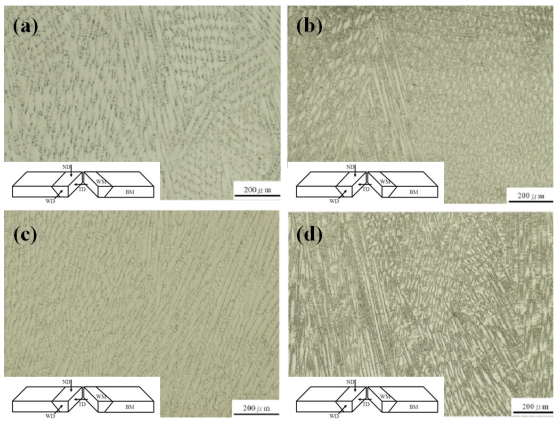

Figure 6. Microstructures of nickel-basesuperalloys in welding direction (WD)

Note: (a) 800H-52 (b) 800H-82 (c) 825-52 (d) 825-82 with an etchant of the Aqua regia plus Glycerin

DOI: https://doi.org/10.30564/jmmr.v2i1.958

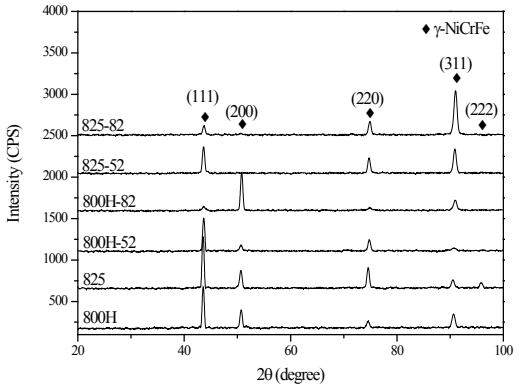

Figure 7. XRD diffraction pattern of nickel-base superalloys

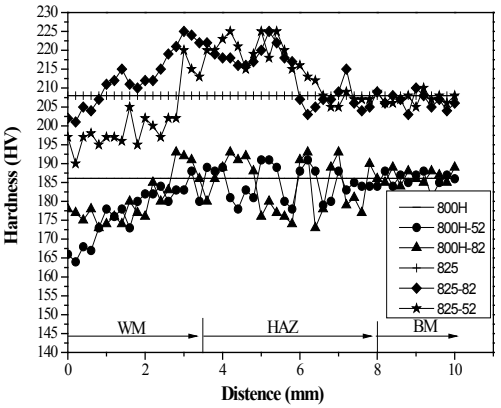

Figure 8. Vickers hardness of nickel-basesuperalloys

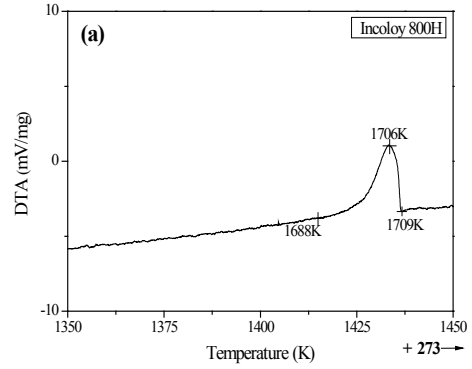

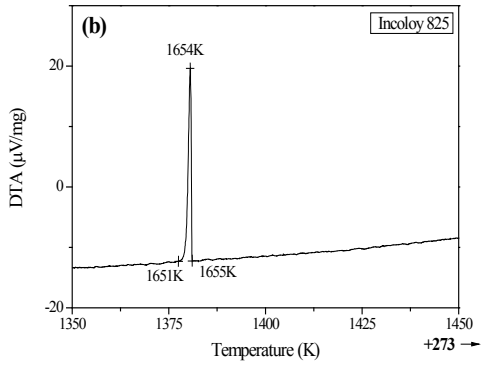

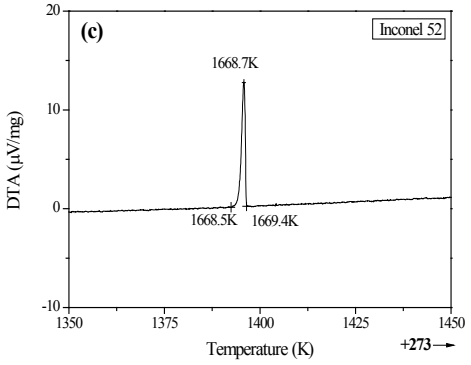

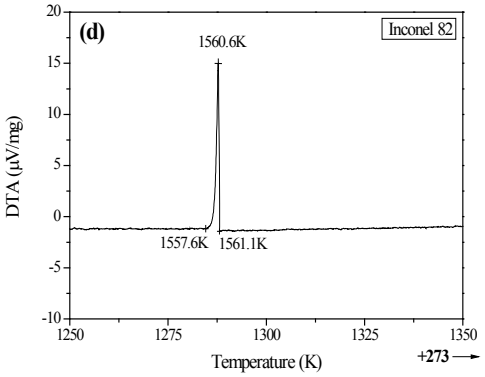

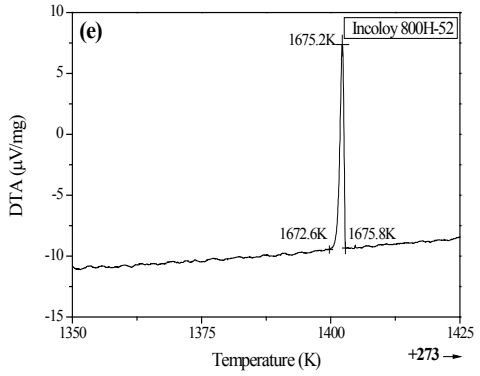

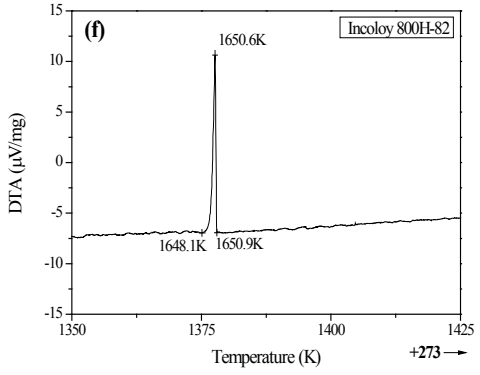

 DOI: https://doi.org/10.30564/jmmr.v2i1.958

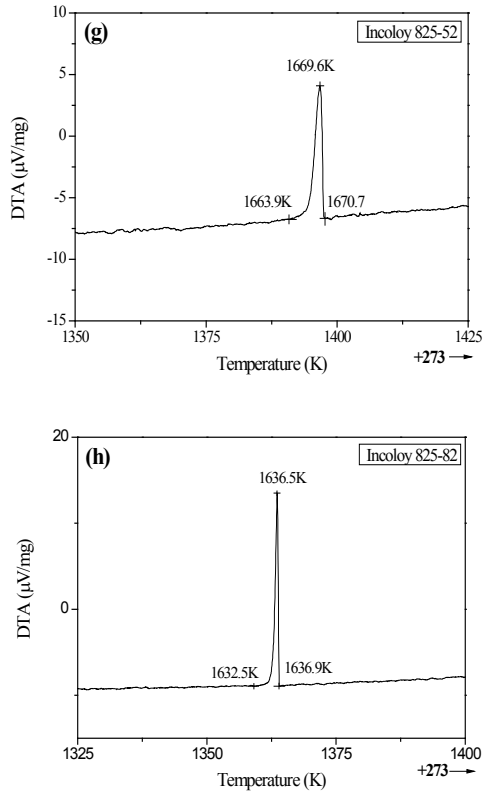

Figure 9. DTA thermal analysis of nickel-basesuperalloys

Note: (a) 800H (b) 825 (c) 52 filler (d) 82 filler (e) 800H-52 (f) 800H-82 (g) 825-52 (f) 825-82

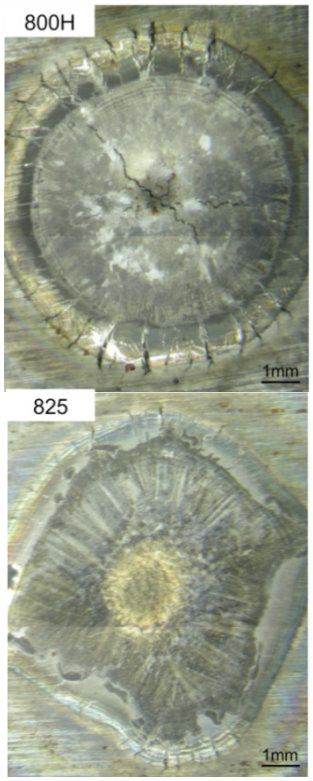

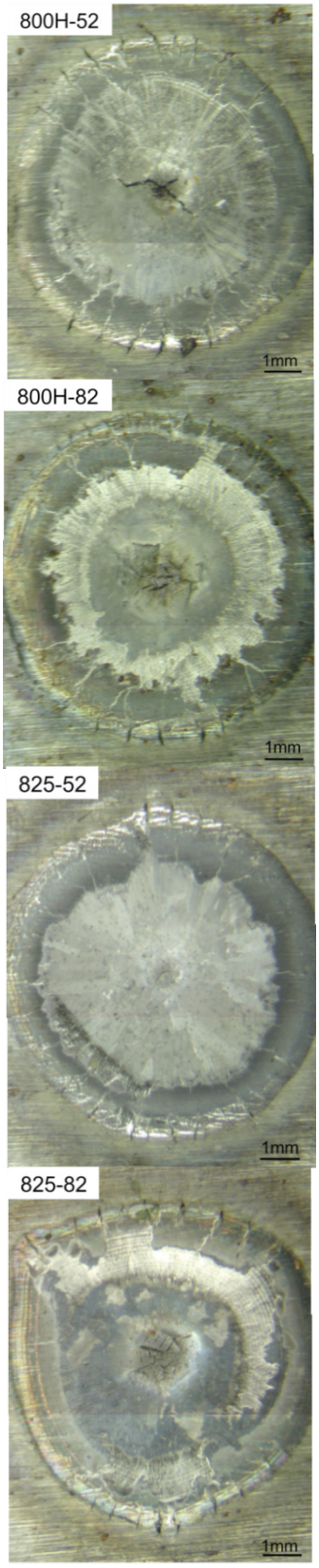

Figure 10. Macrostructures of cracks after Spot Varestraint test

DOI: https://doi.org/10.30564/jmmr.v2i1.958

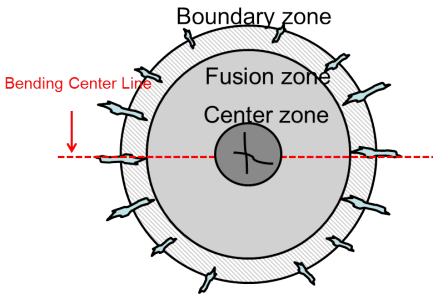

Figure 11. Schematic diagram showing the welding zones after Spot Varestraint test

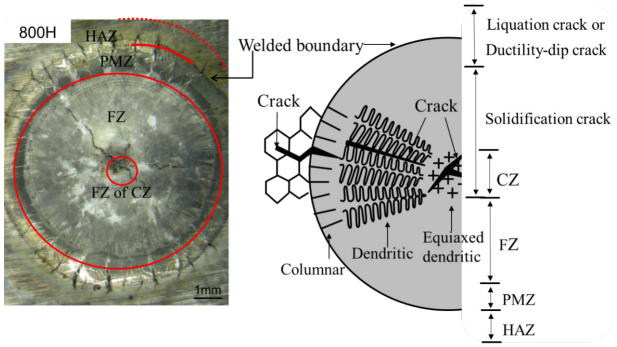

Figure 12. Schematic diagram showing the crack growth and crack mode in nickel-base superalloys

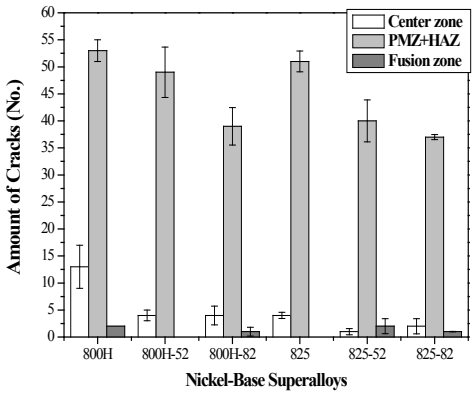

Figure 13. Amount of cracks in nickel-base superalloys

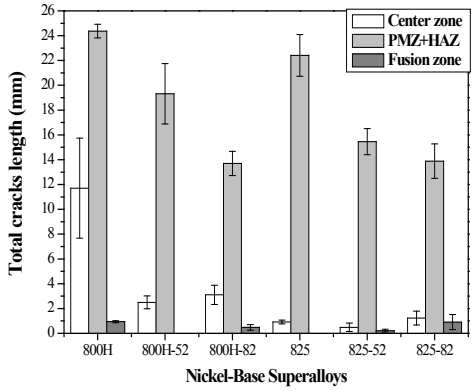

Figure 14. Total cracks length in nickel-base superalloys

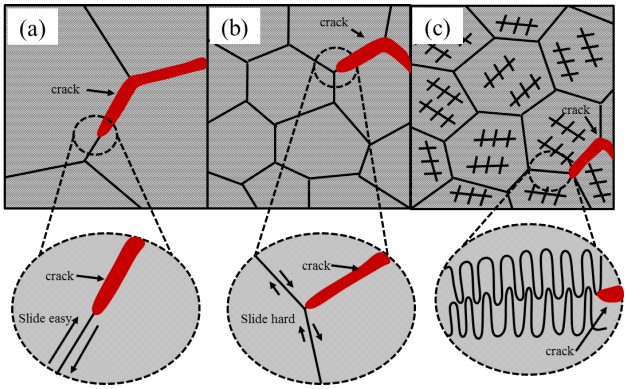

Figure 15. Microstructural development of cracks in nickel-base superalloys

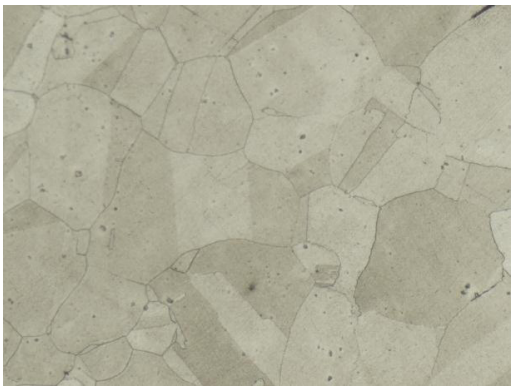

(a)

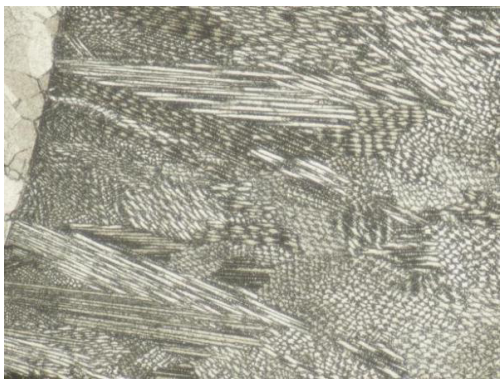

(b)

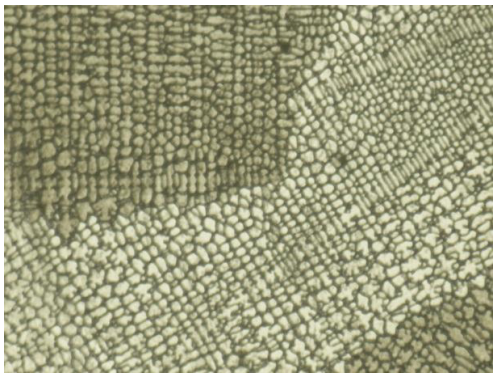

(c)

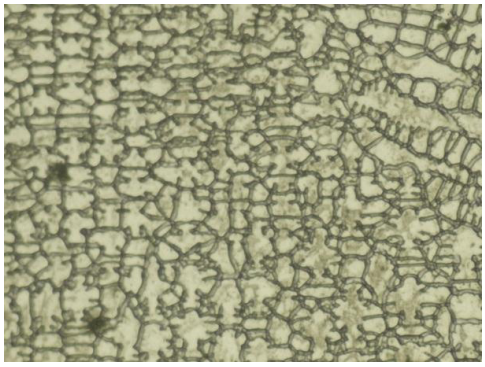

(d)

Figure 16. Microstructures of Spot Varestraint test in different regions

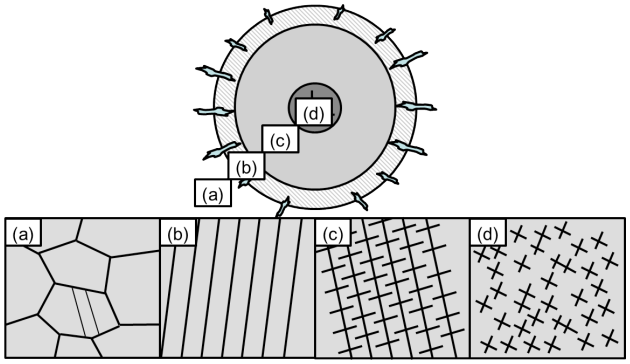

Figure 17. Schematic diagram showing the microstructures in different regions after Spot Varestraint test

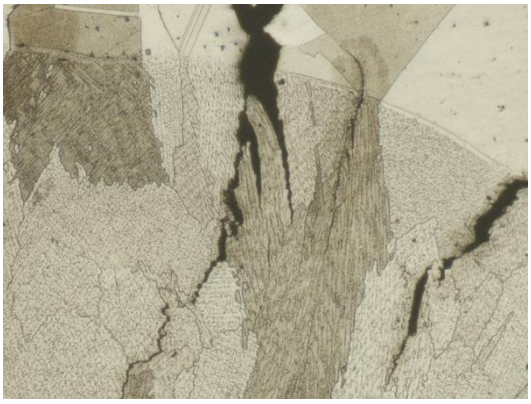

(a)

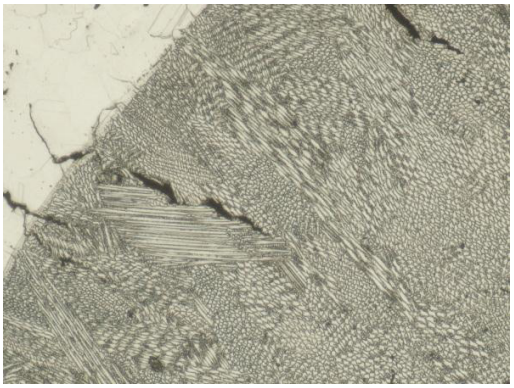

(b)

(c)

(d)

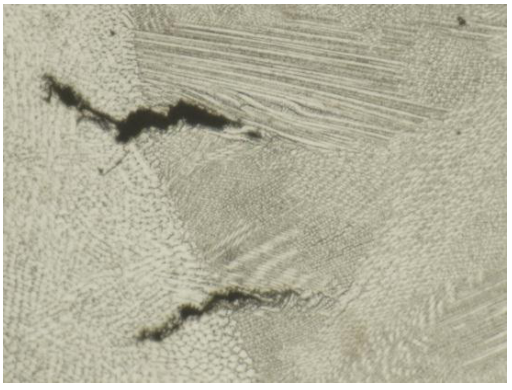

(e)

DOI: https://doi.org/10.30564/jmmr.v2i1.958

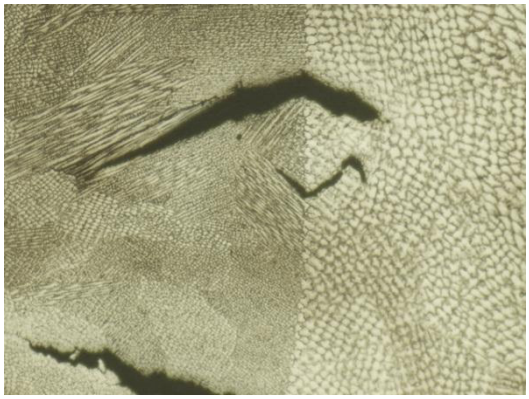

(f)

Figure 18. Metallographic micrographs of cracks in nickel-base superalloys

Note: (a) 800H, (b) 825, (c) 800H-52, (d) 825-52, (e) 800H-82, (f) 825-82

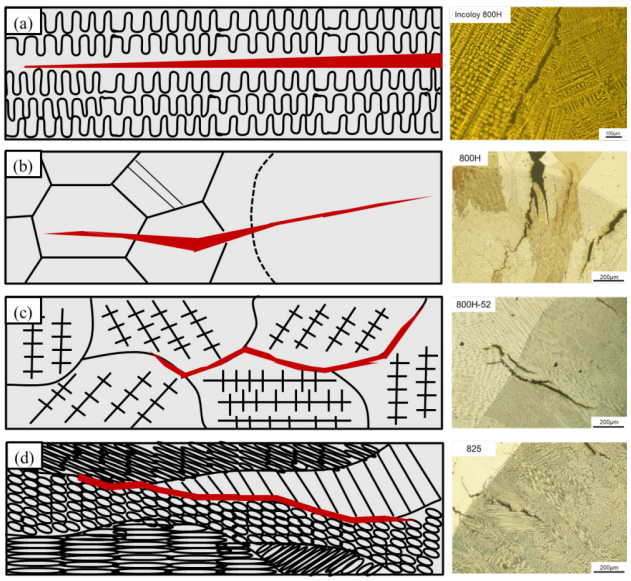

Figure. 19 Different growth modes of cracks in different nickel-base superalloys

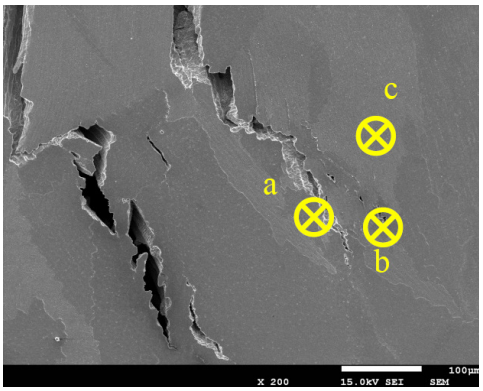

(a)

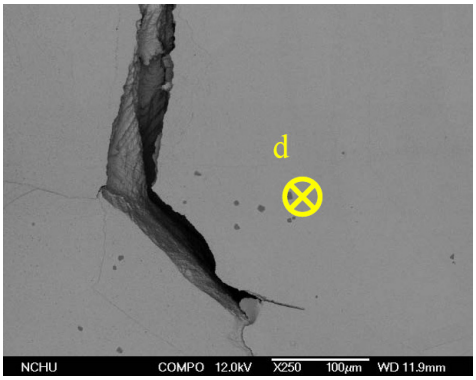

(b)

Figure 20. SEM micrographs in surrounding cracks (a) starting point, (b) terminal point

References

[1] R.A. Page: Corrosion, 1983, 39(21): 409.
[2] R.A. Page and A. McMinn: EPRI NP-5882M Project 1566-1 Final Report, 1988.
[3] H.C. Burghard and A.J. Bursle: SWRI Project 02-5839-001 Final Report, 1978.
[4] P.A. Kammer, K. Masubuchi, and R.E. Monroe: Defense Metals Information Center, DMIC Report 197, 1964.
[5] B. Hemsworth, T. Boniszewski, and N.F. Eation: Metal Const. Br. Weld. J., 1969, 2: 5-16.
[6] X. Ye, X.M. Hua, Y.X. Wu, and S.N. Lou: J Mater. Process Technol., 2015, 217: 13-20.
[7] C. Bellot and P. Lamesle: J. Alloy Compd., 2013, 570: 100-03.
[8] N.R. Sun, L.T. Zhang, Z.G. Li, and A.D. Shan: Mater. Sci. Eng. A, 2014, 606: 417-25.
[9] Y.N. Li, X.S. Liu, J.C. Yang, M. Lin, L. C.F. Li: Mater. Design, 2012, 35: 303-09.
[10] J. Zhang: Scripta Mater., 2003, 48(81): 677.
[11] Y.P. Mei, Y.C. Liu, C.X. Liu, C. Li, L.M. Yu, Q.Y. Guo, and H.J. Li: Mater. Design, 2016, 89(77): 964.
[12] M.T. Rush, P.A. Colegrove, Z. Zhang, and B. Courtot: Adv. Mater. Res., 2010, 89-91(72): 467.
[13] C.P. Chou and C.H. Chao: REPAIR WELDABILITY STUDIES OF ALLOY 718 USING VERSATILE VARESTRAINT TEST, Superalloys, The Metallurgy Society, 1988(93): 785.
[14] C.M. Cheng, C.P. Chou, I.K. Lee, and I.C.Kuo: J. Mater. Sci. Technol., 2006, 22: 685-690.
[15] C.C. Chang, C.L. Chen, J.Y. Wen, C.M. Cheng, and C.P. Chou:Mater. Manuf. Process, 2012, 27(63): 658.
[16] W. Wu and C.H. Tsai: Metall. Mater. Trans. A, 1999, 30(26): 417.

 DOI: https://doi.org/10.30564/jmmr.v2i1.958